domain is connected to the middle domain by a DAO (double crossover with antiparallel helices whose crossovers are separated by an odd number of DNA half-turns) linkage (*3*). In contrast, the central domain is connected to the upper domain by a PX linkage (*7*). Further right on the upper domains, the double-helical continuity is interrupted by a pair of set strands (green in A and B, purple in C and D) that controls the state of the PX-JX_2 device. Proceeding to the right, the two-helix motif continues for about four double-helical turns. A long reporter hairpin has been attached so that it extends perpendicular to the plane of the cassette. This hairpin points in opposite directions in the PX state and in the JX_2 state, enabling differentiation of the two states by means of AFM. The stability of the cassette in both states, with and without the reporter hairpin, is indicated by the presence of single bands on a nondenaturing gel in Fig. 1E.

A three-domain tile (TX) array (*8*) was selected for insertion. In this array, the TX tiles are connected so that the bottom domain of each tile is attached to the upper domain of a tile in an adjacent column (Fig. 2). This arrangement produces slots that may be flanked by sticky ends on the termini of the middle domains of each TX tile. These sticky ends can be used to bind another tile with complementary sticky ends in that site (*8*). We form the TX array with eight unique tiles, so as to accommodate the cassette's long reporter hairpin (Fig. 1); the size of the hairpin needed to demonstrate motion has limited us to only two inserted elements. One of these elements is the cassette, containing the PX-JX_2 device, and the other is a TX marker tile, parallel to the cassette, that enables us to establish a reference frame on the array. The marker tile is in the same column as the cassette insertion domain (Fig. 2). The sequences of the cassette and the tiles are shown in fig. S1; the presence of all strands in each state is shown in figs. S2 and S3; the conversion of state in solution is shown in fig. S4 (*9*).

The results of insertion and state conversion are shown by AFM in Fig. 3. Fig. 3A shows an array of PX-state cassettes (left) that have been converted to JX_2-state cassettes (right); Fig. 3B shows the reverse conversion, where an array formed with JX_2-state cassettes (left) is converted to cassettes in the PX state (right). It is important to recognize that these conversions occur after the cassettes have been inserted into the array [detailed methods are described in (*9*)]. In addition to the arrays shown in Fig. 3, we have examined two other sets of inserted cassette arrays (figs. S5 and S6) (*9*). As summarized in table S1 (*9*), the AFM images are only good enough to ascertain the states of about half of the pretransition cassettes and slightly fewer of the posttransition cassettes. Among the three image sets (Figs. 3 and figs. S5 and S6), we detected no errors in the pretransition arrays. After conversion from the PX state, 95 of 96 cassettes are seen correctly in the JX_2 state; after conversion from the JX_2 state, 85 of 86 cassettes are seen correctly in the PX state, suggesting a conversion error rate ~1%.

It is crucial for nanorobotics to be able to insert controllable devices into a substrate, thereby leading to a diversity of structural states. Here we have demonstrated that a single device has been inserted and converted at a specific site. There is no reason to expect that the system is limited to a single device unit; as noted above, the specific addressability of the two-state PX-JX_2 device has been demonstrated previously (*6*). It has been pointed out that two opposing PX-JX_2 devices could be used to produce complex patterns (*10*). The eight-tile TX array used here is technically difficult to obtain, but the recent advance in simplified 2D DNA patterning by Rothemund (*11*) should facilitate the construction of complex base planes for these systems. Similarly, DNA tubes (*12*) provide a means to incorporate nanomechanical devices into nonplanar 2D arrangements.

References and Notes

1. N. C. Seeman, P. S. Lukeman, *Rep. Prog. Phys.* **68**, 237 (2005).
2. H. Qiu, J. C. Dewan, N. C. Seeman, *J. Mol. Biol.* **267**, 881 (1997).
3. T.-J. Fu, N. C. Seeman, *Biochemistry.* **32**, 3211 (1993).
4. E. Winfree, F. Liu, L. A. Wenzler, N. C. Seeman, *Nature* **394**, 539 (1998).
5. H. Yan, X. Zhang, Z. Shen, N. C. Seeman, *Nature* **415**, 62 (2002).
6. S. Liao, N. C. Seeman, *Science* **306**, 2072 (2004).
7. Z. Shen, H. Yan, T. Wang, N. C. Seeman, *J. Am. Chem. Soc.* **126**, 1666 (2004).
8. T. LaBean *et al.*, *J. Am. Chem. Soc.* **122**, 1848 (2000).
9. Materials and methods, additional AFM images, and gel evidence for cassette formation are available as supporting material on *Science* Online.
10. A. Carbone, N. C. Seeman, *Proc. Natl. Acad. Sci. U.S.A.* **99**, 12577 (2002).
11. P. W. K. Rothemund, *Nature* **440**, 297 (2006).
12. W. B. Sherman, N. C. Seeman, *Biophys. J.* **90**, 4546 (2006).
13. J. J. Birac, W. B. Sherman, J. Kopatsch, P. E. Constantinou, N. C. Seeman, *J. Mol. Graph. Model.* **25**, 470 (2006).

14. We thank R. Sha for valuable discussions and C. Mao, H. Yan, and N. Jonoska for useful comments on the manuscript. This research has been supported by grants from the National Institute of General Medical Sciences, NSF, the Army Research Office, and Nanoscience Technologies. N.C.S. is a scientific advisor to Nanoscience Technologies. Both the PX-JX_2 device and 2D DNA arrays have had patent applications submitted. The 2D arrays are U.S. patent 6,255,469.

Supporting Online Material

www.sciencemag.org/cgi/content/full/314/5805/1583/DC1
Materials and Methods
SOM Text
Figs. S1 to S6
Table S1
References

16 June 2006; accepted 20 October 2006
10.1126/science.1131372

Enzyme-Free Nucleic Acid Logic Circuits

Georg Seelig,[1] David Soloveichik,[2] David Yu Zhang,[2] Erik Winfree[2,3]*

Biological organisms perform complex information processing and control tasks using sophisticated biochemical circuits, yet the engineering of such circuits remains ineffective compared with that of electronic circuits. To systematically create complex yet reliable circuits, electrical engineers use digital logic, wherein gates and subcircuits are composed modularly and signal restoration prevents signal degradation. We report the design and experimental implementation of DNA-based digital logic circuits. We demonstrate AND, OR, and NOT gates, signal restoration, amplification, feedback, and cascading. Gate design and circuit construction is modular. The gates use single-stranded nucleic acids as inputs and outputs, and the mechanism relies exclusively on sequence recognition and strand displacement. Biological nucleic acids such as microRNAs can serve as inputs, suggesting applications in biotechnology and bioengineering.

To date, no man-made chemical circuits even remotely approach the complexity and reliability of silicon-based electronics. Once reliable principles for their design are established, synthetic chemical circuits could be used routinely to control nanoscale devices in vitro, to analyze complex chemical samples in situ, or to interface with existing biological circuits in vivo (*1*). Construction of synthetic biological circuits de novo is a powerful test of design principles (*2*).

Rational design of nucleic acid devices is simplified by the predictability of Watson-Crick base pairing; thus, nucleic acids are a promising alternative to proteins for synthetic chemical circuits. Allosteric ribozymes that take small molecules as input have been shown to perform logical functions (*3*). However, their output (a cleaved or ligated oligonucleotide) is of a different form than the input; hence, cascading is difficult. Automata performing multiple logical operations in parallel (*4*), single-step signaling cascades (*5*),

[1]Department of Applied Physics, California Institute of Technology, Pasadena, CA 91125, USA. [2]Department of Computation and Neural Systems, California Institute of Technology, Pasadena, CA 91125, USA. [3]Department of Computer Science, California Institute of Technology, 1200 East California Boulevard, Pasadena, CA 91125, USA.

*To whom correspondence should be addressed. E-mail: winfree@caltech.edu

and a feedback cycle that acts as an exponential chain reaction (*6*) were built using deoxyribozymes controlled by input oligonucleotides (*7*). Another approach uses sequence recognition to control enzyme catalysis of covalent bond formation and breakage (*8*–*10*). Alternatively, nucleic acid reactions can be driven without enzyme or (deoxy)ribozyme catalysis (*11*, *12*); this principle has been exploited to construct DNA-based logic gates and signaling cascades (*13*, *14*). Such molecular automata may give rise to "smart" therapeutics for medical applications (*7*, *9*, *10*). Recently, engineered nucleic acid logic switches based on hybridization and conformational changes have been successfully demonstrated in vivo (*15*, *16*). The remaining challenge is to design chemical logic gates that can be combined to construct large, reliable circuits. The analogous challenge for engineering electronic circuits was met by the development of digital design principles (*17*); these may also prove essential for designing complex yet robust chemical circuits.

We report the construction of in vitro DNA-based logic gates and circuits that embody digital design principles: logic, cascading, restoration, fan-out, and modularity. These circuits implement a complete set of Boolean logic functions (AND, OR, and NOT) using short oligonucleotides as input and output. Because the input and output are of the same form, the gates can be cascaded to create multilayer circuits. Logical values "0" and "1" are represented by low and high concentrations, respectively. Signal restoration is performed by threshold and amplifier gates that protect against noise, signal loss, and leaky reactions. Amplifier gates can also be used to ensure that a logic gate generates sufficient signal to drive multiple downstream targets. Watson-Crick interactions between modular recognition domains determine the connectivity of gates. Sequences can be chosen with few constraints, allowing the construction of arbitrary circuits with negligible cross-activation. Furthermore, modular construction allows for interfacing with existing molecular components—be they predesigned subcircuits or naturally occurring nucleic acids.

Gate function is entirely determined by base pairing and breaking. Every gate consists of one or more gate strands and one output strand (Fig. 1A and fig. S1). The output strand either serves as an input to a downstream gate or is modified with a dye label to provide a readout in a fluorescence experiment. Both ends of the output strand (Fig. 1A), or only one end (translator gates in Fig. 2), can be attached to the gate complex. Figure 1A shows an AND-gate assembled from an output strand and two gate strands. The addition of single-stranded inputs to a solution containing the gate initiates a computation. Each gate strand contains a recognition region that is complementary to its input. Initially, the recognition regions of all gate strands are double-stranded and therefore inert, except for the toehold farthest from the output strand (strand G in Fig. 1A). When the first input binds this toehold, it displaces the first gate strand by three-way branch migration (*18*, *19*), exposing the toehold for the subsequent input and releasing an inert double-stranded waste product. A similar process can now occur for the second input. The output strand is released if and only if both inputs are present. To implement this design, DNA sequences (tables S1 to S3) were selected to ensure correct complementarity while minimizing spurious interactions (*20*).

The two-input AND gate has four entries in its truth table (Fig. 1B) and was shown to function correctly when tested by fluorescence kinetics experiments and gel electrophoresis (Fig. 1, C and D). We also designed multi-input AND gates using the same principles and showed that they work reliably (fig. S2). The gates in all of our experiments were purified by gel electrophoresis after triggering "leaky" complexes (*20*) (fig. S3).

The output strand of one gate may be an input strand to a downstream gate. It is essential that the output strand not interact with downstream gates before release. Protecting the toehold binding region of output strands in upstream gates prevents such interactions. We built a circuit composed of one AND gate and two translator gates that demonstrates this principle (Fig. 2A and fig. S4). A translator gate converts the signal encoded in the input strand to the signal encoded in the output strand and is implemented as a single-input AND gate. The translator gates JK and LM translate two biological microRNA sequences (mouse let-7c and miR-124a) into outputs with recognition regions identical to strands G_{in} and F_{in}. The input to a translator gate and the recognition region of its output strand need only share sequence in the toehold region. If two translators are cascaded, then there is no sequence restriction between the initial input strand and the final output strand. This is called a full translator; the cascading of NO and HI is an example (Fig. 3 and fig. S1). Translators can connect subcircuits that do not a priori use the same sequences for the

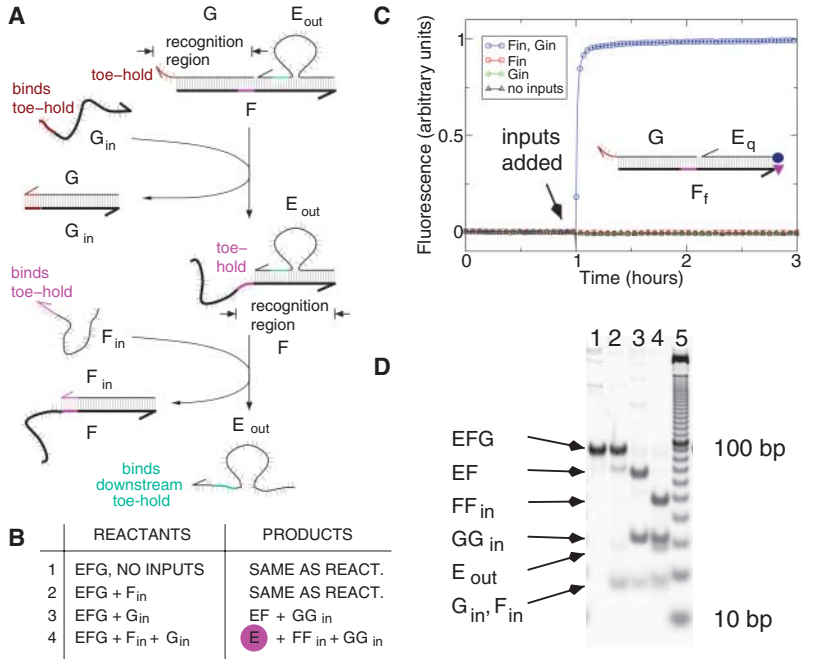

Fig. 1. Two-input AND gate. (**A**) The gate consists of three DNA strands, E_{out} [57 nucleotides (nt)], F (60 nt), and G (36 nt). The 3′ ends are marked by arrows. Toeholds and toehold binding regions (all six nucleotides) are indicated in color. Input strands F_{in} and G_{in} (36 nt) are complementary to recognition regions within the corresponding gate strands F and G. (**B**) Truth table for the two-input AND gate. The released output strand is highlighted. (**C**) In fluorescence experiments, strands F_f [carboxytetramethylrhodamine (TAMRA) fluorophore at the 3′ end] and E_q (Iowa Black RQ quencher at the 5′ end, without bulge loop) were used instead of F and E_{out} (see inset). Release of output strand results in increased fluorescence. Experiments were conducted at 25°C with gate concentrations of 250 nM and input concentrations of 300 nM in a Tris-acetate-EDTA buffer containing 12.5 mM Mg^{++}. (**D**) Nondenaturing gel electrophoresis directly confirms reaction intermediates and waste products for each possible input combination. Lanes 1 to 4: The samples are as described in entries 1 to 4 of the truth table. The gate used in this experiment is as shown in (A). Lane 5: 10–base pair (bp) ladder.

toehold and recognition regions. This is particularly useful for adapting an existing circuit to compute on arbitrary biological inputs.

The circuit of Fig. 2A was also tested under conditions relevant to potential biological applications. The circuit works comparably with RNA inputs as with DNA inputs because gate function depends solely on Watson-Crick complementarity (Fig. 2A and fig. S4). Increasing the temperature to 37°C does not degrade circuit performance. Finally, the circuit functions well in the presence of potentially interfering biological RNA (mouse brain total RNA) at a concentration in excess of gate complexes and input strands.

Because a small set of logic gates (AND, OR, and NOT) is sufficient for effective computation of any Boolean function, we developed DNA gates to perform these operations. Logical OR functionality is obtained by using two gates that produce the same output. We constructed a three-gate chemical circuit in which a logical OR feeds into a logical AND (fig. S4B). Acting as a logical OR, translator gates ST and UV take different inputs (miR-15a and miR-10b) but release outputs with identical recognition regions. If Boolean values are represented by the presence of either one strand ("0") or another strand ("1")—the so-called "dual-rail" representation (*21*)—then AND and OR are themselves sufficient to compute any Boolean function.

If a Boolean value is represented by the presence or absence of a single input strand, a NOT gate may be necessary. We modified the circuit shown in Fig. 2A to invert the let-7c input (Fig. 2B). The NOT gate makes use of an additional "inverter" strand that triggers the gate unless the input strand is present to act as a competitive inhibitor. Because the inverter strand must be added simultaneously with the input, NOT gates are restricted to the first layer of the circuit. This is sufficient to create a dual-rail representation from which arbitrary subsequent computation can be performed with just AND and OR.

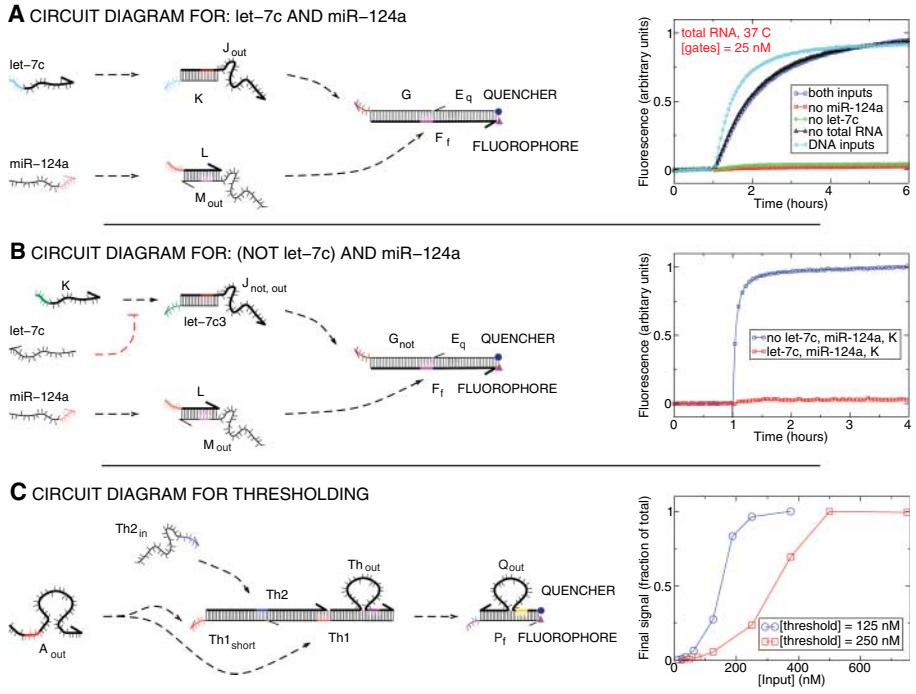

Fig. 2. Translator gates, NOT operation, and signal restoration. Dashed arrows indicate where input or output strands can serve as inputs to downstream gates. (**A**) Circuit operation at 37°C with RNA inputs and DNA gates in a total RNA background. All gates are at 25 nM, synthetic RNA inputs are at 30 nM, and total RNA (mouse brain) is at a concentration of 200 μg/ml. Proper function is observed. For comparison, experiments with no total RNA were performed, using either both RNA inputs or both DNA inputs. (**B**) The NOT gate consists of a translator gate and an inverter strand complementary to let-7c. Gate, inverter strand, and input concentrations are 250 nM, 300 nM, and 300 nM, respectively. Here and in all subsequent experiments, the temperature was 25°C and DNA equivalents of the biological microRNAs were used. If let-7c was present, inverter strand K preferentially hybridized to let-7c. Otherwise, inverter strand K triggered the translator. (**C**) The thresholding gate, using a dye/quencher-labeled readout gate to monitor the output. Strand $Th2_{in}$ is part of the thresholding unit and was added before the start of the experiment. The final fluorescence is plotted against the input concentration for two different concentrations of the threshold gate.

A gate may fail in two ways: It may fail to produce enough output when triggered, or it may "leak" by spontaneously releasing the output strand. Both types of error require signal restoration; the former requires increasing a moderate output amount to the full activation level, and the latter requires decreasing a small output amount to a negligible level. To implement signal restoration, we developed gates for amplification and thresholding. The threshold gate (Fig. 2C) is a three-input AND gate with identical first and third inputs. The second input is only necessary for structural purposes; it is always present and can be considered part of the thresholding unit. A substoichiometric amount of input (with respect to threshold gates) will cause most gates to lose only their first and second gate strands, thus releasing no output. Input concentrations two times as high as the concentration of threshold gates will cause most gates to produce output. The threshold gate's concentration sets the threshold for a sigmoidal nonlinearity (Fig. 2C and fig. S5) (*20*).

Because the threshold gate's output cannot exceed half the input signal, subsequent amplification is necessary. A hybridization-based system for catalytic amplification was demonstrated previously (*22*). With minor modifications, the system serves as both an input amplifier and full translator (fig. S6 and Fig. 3, left, miR-143 translator), or as a fluorescence readout (fig. S7A and Fig. 3, right). Alternatively, amplifiers based on feedback logic can be designed (fig. S6B). A threshold gate together with an amplifier gate constitutes a signal restoration module whose incorporation into large circuits at multiple intermediate points ensures the stability of digital representation (*23*).

Finally, to demonstrate modularity and scalability, we composed eleven gates into a larger circuit. The circuit combines previously introduced modules for input translation and amplification, calculation of AND and OR, and signal restoration (Fig. 3). The inputs to the circuit are DNA analogs of six mouse microRNAs. To determine the effectiveness of signal restoration, we constructed an equivalent circuit without signal restoration and tested both circuits with an input at one-quarter the strength of a signal that is fully on (0.25×) to simulate a large upstream leak. The complete circuit maintained a low output signal, whereas the circuit without signal restoration exhibited a ≈25% output leak (Fig. 3, inset). To verify other circuit components, several subcircuits were constructed and tested independently (figs. S8 and S9). The feedback fluorescence amplifier was tested as a replacement for the catalytic amplifier at the output, resulting in a circuit containing 12 gates (fig. S10).

As increasingly larger circuits are constructed, speed becomes a limiting factor. The circuit without signal restoration takes 2 hours

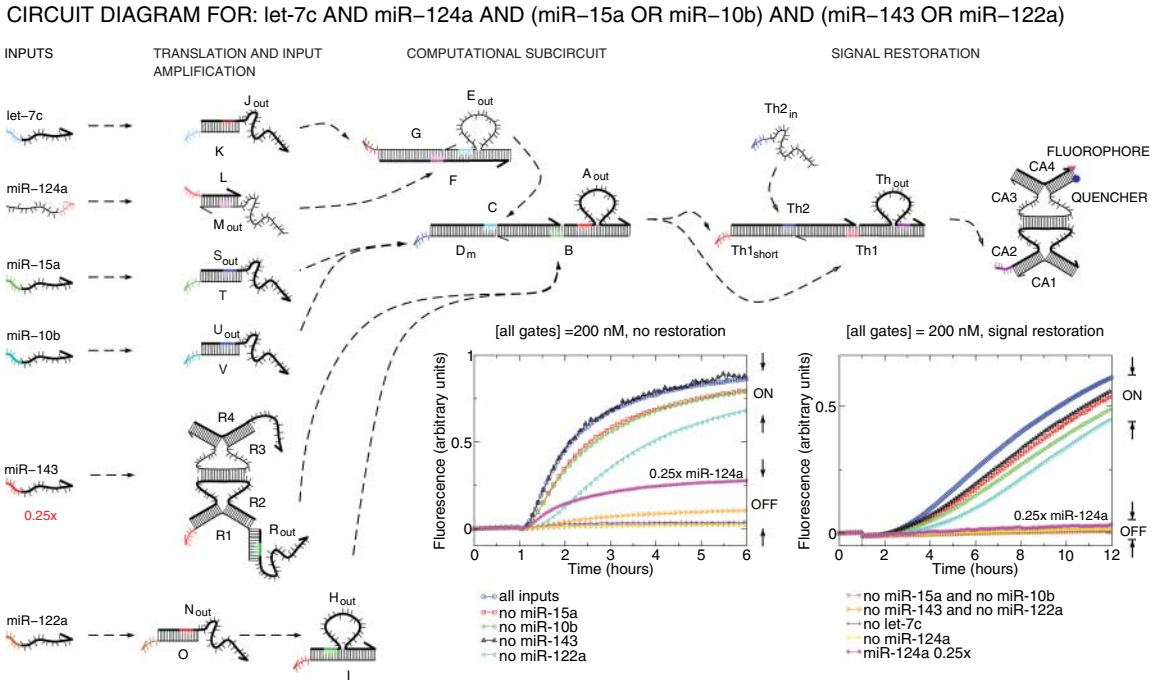

Fig. 3. Signal propagation through a complex chemical circuit combining AND, OR, sequence translation, input amplification, and signal restoration. The five-layer circuit consists of a total of 11 gates and accepts six inputs. With the exception of the threshold gate, which was at 100 nM with its $Th2_{in}$ strand at 150 nM, all gates were at 200 nM (1×) per gate. Unless otherwise specified, inputs were added at 250 nM (1.25×). miR-143 was added at 50 nM (0.25×) and subsequently amplified by the input amplifier. (Inset) Fluorescence traces of circuit operation without and with the signal restoration module (threshold plus amplifier). The traces for input conditions corresponding to a logical TRUE output (ON) are clearly distinguishable from the logical FALSE output (OFF). Cases tested include when all inputs are present, all cases in which exactly one input is missing, and combinations of inputs that turn off an OR clause. Assuming monotonicity, withholding additional inputs will never lead to a logical TRUE output. To determine the response of the circuit to a leaky OFF signal, input miR-124a was added at 50 nM (0.25×) while all other inputs were added normally.

to reach half-activation (Fig. 3, left inset). The circuit with signal restoration has two additional layers and takes 10 hours to achieve half-activation (Fig. 3, right inset). Despite the slow operation, in both cases a clear difference between off and on states can be distinguished much earlier. Speeding up the responses of individual gates (e.g., by shortening recognition domains) or changing other reaction conditions may improve overall circuit performance.

Our success in creating large circuits can be attributed to adherence to the tenets of digital logic, toehold sequestering combined with branch migration and strand displacement, reduction of leak reactions by purification, and modularity of design. The logic gates developed here and the principles on which they are based can also be used to construct analog or hybrid circuits (*24*) and are likely to prove compatible with other approaches to building molecular automata in vitro and in vivo (*5*, *7*–*9*, *13*, *15*, *16*). Because evidence suggests that our logic gates can use natural RNA as input and that they behave correctly in the presence of mouse total RNA, our hybridization-based circuits might be adapted for in situ detection of complex expression patterns or even in vivo logic processing.

References and Notes

1. F. J. Isaacs, D. J. Dwyer, J. J. Collins, *Nat. Biotechnol.* **24**, 545 (2006).
2. D. Sprinzak, M. B. Elowitz, *Nature* **438**, 443 (2005).
3. R. R. Breaker, *Curr. Opin. Biotechnol.* **13**, 31 (2002).
4. M. N. Stojanovic, D. Stefanovic, *Nat. Biotechnol.* **21**, 1069 (2003).
5. R. Penchovsky, R. R. Breaker, *Nat. Biotechnol.* **23**, 1424 (2005).
6. M. Levy, A. D. Ellington, *Proc. Natl. Acad. Sci. U.S.A.* **100**, 6416 (2003).
7. M. N. Stojanovic, T. E. Mitchell, D. Stefanovic, *J. Am. Chem. Soc.* **124**, 3555 (2002).
8. Y. Benenson, T. Paz-Elizur, R. Adar, E. Keinan, E. Shapiro, *Nature* **414**, 430 (2001).
9. Y. Benenson, B. Gil, U. Ben-Dor, R. Adar, E. Shapiro, *Nature* **429**, 423 (2004).
10. B. Yurke, A. P. Mills Jr., S. L. Cheng, *Biosystems* **52**, 165 (1999).
11. B. Yurke, A. J. Turberfield, A. P. Mills Jr., F. C. Simmel, J. L. Neumann, *Nature* **406**, 605 (2000).
12. A. J. Turberfield *et al.*, *Phys. Rev. Lett.* **90**, 118102 (2003).
13. M. Hagiya, S. Yaegashi, K. Takahashi, in *Nanotechnology: Science and Computation,* J. Chen, N. Jonoska, G. Rozenberg, Eds. (Springer-Verlag, Berlin, Germany, 2006), pp. 293–308.
14. R. M. Dirks, N. A. Pierce, *Proc. Natl. Acad. Sci. U.S.A.* **101**, 15275 (2004).
15. F. J. Isaacs *et al.*, *Nat. Biotechnol.* **22**, 841 (2004).
16. T. S. Bayer, C. D. Smolke, *Nat. Biotechnol.* **23**, 337 (2005).
17. In contrast to digital electronic circuits, analog electronic circuits have not advanced rapidly because circuit design remains more "art" than systematic engineering, making the construction of large reliable circuits difficult. This is often attributed to the lack of the digital abstraction: In analog circuits even slight signal changes carry meaning (e.g., the value is 5.2 not 5.3) and thus restoration to clean up noise or gate malfunction is not possible. The lack of restoration also complicates circuit modularity, because circuit behavior can be subtly changed when subcircuits are combined (*24*).
18. C. S. Lee, R. W. Davis, N. Davidson, *J. Mol. Biol.* **48**, 1 (1970).
19. B. Yurke, A. P. Mills Jr., *Genet. Program. Evolvable Mach.* **4**, 111 (2003).
20. Materials and methods are available as supporting material on *Science* Online.
21. D. E. Muller, in *Application of Switching Theory in Space Technology*, H. Aiken, W. F. Main, Eds. (Stanford Univ. Press, Stanford, CA, 1963), pp. 289–297.
22. G. Seelig, B. Yurke, E. Winfree, *J. Am. Chem. Soc.* **128**, 12211 (2006).
23. J. von Neumann, in *Automata Studies*, C. Shannon, J. McCarthy, Eds., vol. 34 of *Annals of Mathematical Studies* (Princeton Univ. Press, Princeton, NJ, 1956), pp. 43–98.
24. R. Sarpeshkar, *Neural Comput.* **10**, 1601 (1998).

25. We thank N. Dabby for a very close reading of this paper and extensive revisions. B. Yurke built the custom fluorometer used for these experiments, and we are further indebted to him for inspiration and advice. G.S. was supported by the Swiss National Science Foundation, the Center for Biological Circuit Design at the California Institute of Technology, and the NSF grant CHE-0533065 (Chemical Bonding Center) to M. N. Stojanovic. E.W. acknowledges NSF awards no. 0093846 and no. 0506468, and Human Frontier Science Program award no. RGY0074/2006-C.D.S. and D.Y.Z. were partially supported by a National Institute of Mental Health Training Grant to the Computation and Neural Systems option at the California Institute of Technology. D.Y.Z. was partially supported by a California Institute of Technology Grubstake award.

Supporting Online Material

www.sciencemag.org/cgi/content/full/314/5805/1585/DC1
Materials and Methods
Figs. S1 to S10
Tables S1 to S3

14 July 2006; accepted 13 November 2006
10.1126/science.1132493

Enzyme-Free Nucleic Acid Logic Circuits

Georg Seelig, David Soloveichik, David Yu Zhang and Erik Winfree

Science **314** (5805), 1585-1588.
DOI: 10.1126/science.1132493